Published in final edited form as:

Proc SPIE Int Soc Opt Eng. 2012 February 4; 8316: . doi:10.1117/12.912869.

Calibration and Evaluation of a Magnetically Tracked ICE Probe for Guidance of Left Atrial Ablation Therapy

Cristian A. Linte[a,b], **Maryam E. Rettmann**[a,b], **Ben Dilger**[d], **Mia S. Gunawan**[e], **Shivaram Poigai Arunachalam**[b], **David R. Holmes III**[a,b], **Douglas L. Packer**[c], and **Richard A. Robb**[a,b]

[a]Biomedical Imaging Resource, Mayo Clinic, Rochester, MN, USA

[b]Department of Physiology and Biomedical Engineering, Mayo Clinic, Rochester, MN, USA

[c]Division of Cardiology, Mayo Clinic, Rochester, MN, USA

[d]Carver College of Medicine, University of Iowa, Iowa City, IA, USA

[e]Department of Biochemistry and Molecular & Cellular Biology, Georgetown University Medical Center, Washington, DC, USA

Abstract

The novel prototype system for advanced visualization for image-guided left atrial ablation therapy developed in our laboratory permits ready integration of multiple imaging modalities, surgical instrument tracking, interventional devices and electro-physiologic data. This technology allows subject-specific procedure planning and guidance using 3D dynamic, patient-specific models of the patient's heart, augmented with real-time intracardiac echocardiography (ICE). In order for the 2D ICE images to provide intuitive visualization for accurate catheter to surgical target navigation, the transducer must be tracked, so that the acquired images can be appropriately presented with respect to the patient-specific anatomy. Here we present the implementation of a previously developed ultrasound calibration technique for a magnetically tracked ICE transducer, along with a series of evaluation methods to ensure accurate imaging and faithful representation of the imaged structures. Using an engineering-designed phantom, target localization accuracy is assessed by comparing known target locations with their transformed locations inferred from the tracked US images. In addition, the 3D volume reconstruction accuracy is also estimated by comparing a truth volume to that reconstructed from sequential 2D US images. Clinically emulating validation studies are conducted using a patient-specific left atrial phantom. Target localization error of clinically-relevant surgical targets represented by nylon fiducials implanted within the endocardial wall of the phantom was assessed. Our studies have demonstrated 2.4 ± 0.8 mm target localization error in the engineering-designed evaluation phantoms, 94.8 ± 4.6 % volume reconstruction accuracy, and 3.1 ± 1.2 mm target localization error in the left atrial-mimicking phantom. These results are consistent with those disseminated in the literature and also with the accuracy constraints imposed by the employed technology and the clinical application.

Further author information: Cristian A. Linte (linte.cristian@mayo.edu); Richard A. Robb (robb.richard@mayo.edu), Biomedical Imaging Resource, Mayo Clinic: 200 First Street SW, Rochester, MN, 55902.

Keywords

Image-Guided Cardiac Procedures; Intra-operative Imaging; Ultrasound Guidance; Localization and Tracking Technologies; Calibration

1. INTRODUCTION

Catheter-based ablation therapy for treatment of arrhythmias has received extensive attention over the past decade and success rates as high as 80% have been demonstrated possible for treatment of certain arrhythmic conditions. However, the more common 40–60% success rates associated with such treatments have come at a high price, including lengthy procedures accompanied by extensive exposure to ionizing radiation and unacceptably high intervention risks.[1] Several groups have reported the incorporation of 3D images and models generated from pre-operative CT[2] or MR scans[3] into the procedure. Their emphasis has been to create detailed patient-specific visualizations that can be registered to the intra-operative fluoroscopy images,[4] with the eventual goal of reducing or eliminating dose exposure. However, the models are generated at one instant in time, are available for review during the procedure, but have no direct relationship with the intra-operative guidance environment.

As a significant and unique solution to these limitations, a novel prototype system for advanced visualization for image-guided left atrial ablation therapy has been developed in our laboratory.[5] This technology permits ready integration of multiple imaging modalities, surgical instrument tracking, interventional devices and electrophysiologic data, and allows subject-specific procedure planning and guidance using 3D dynamic, patient-specific cardiac models obtained from high-quality, pre-operative tomographic images (Fig. 1). Direct imaging using intracardiac ultrasound (US) has also shown promise as an on-line means of visualizing specific cardiac structures within their surrounding anatomical context and guiding catheter tip in contact with the endocardial surface.[6]

This work complements our previous efforts and focuses on the intra-operative imaging aspect of the platform. Real-time imaging is crucial for intra-procedure visualization and intracardiac echocardiography (ICE) is standard of care for intra-operative left atrial imaging and catheter guidance. The ICE probe is introduced through the vasculature into the right atrium and used to acquire images of the "surgical scene" in the left atrium. To ensure accurate and intuitive visualization during therapy delivery, the US fan must be tracked, so that the acquired images can be presented in the context of the patient-specific anatomy. Hence, the accuracy of the tracking sensor-to-transducer calibration significantly influences the quality of all subsequent US-based measurements. Here we describe an evaluation methodology conducted *in vitro* employing both engineering-designed phantoms as well as a left-atrial emulating phantom to ensure that the implemented calibration technique performs adequately for this application.

2. METHODOLOGY

2.1. Probe Calibration

It is generally accepted that optical tracking systems have established the "gold-standard" for accuracy in the OR and can produce tracking accuracy on the order of 0.1–0.3mm.[7, 8] However, when the tracked object is at the end of a flexible cable inside the body, optical systems cannot be used because of the lack of line-of-sight between the transmitter and receiver. Instead, magnetic tracking systems[9] (MTS) are employed.

For this application the NDI Aurora (Northern Digital Inc., Waterloo, Canada) MTS available in our laboratory was employed. A 6D magnetic sensor coil was rigidly attached to the ICE transducer; the position and orientation of the assembly is determined based on the eddy currents induced in the coil and it is dependent on its pose within the magnetic field produced by the field generator.

A standard calibration technique[10] was employed, in which a Z-string phantom (a phantom containing 4 Z-string patterns) of known geometrical properties was scanned with the tracked US probe. For each acquired image, the intersection of the imaginary US image plane with the physical strings forming the Z-patterns produces a unique configuration of the string traces (bright dots) in the US image. The calibration is performed by determining the transformation that minimizes the distance between features in the US images and the actual phantom[11,12] using a least-square solution. Once this transformation is determined, any subsequent measurements made or features identified in the acquired US images can be mapped into the global coordinate system by means of the calibration transform and respective pose of the US transducer.

The sensor tool-to-US probe calibration transform $\left[\mathrm{T}_{US}^{tool}\right]$ is determined from the following relationship: $\left[\mathrm{T}_{ph}^{EM}\right]\cdot\{\mathrm{X}_{ph}\}=\left[\mathrm{T}_{tool}^{EM}\right]\cdot\left[\mathrm{T}_{US}^{tool}\right]\cdot\{\mathrm{X}_{US}\}$, where $\left[\mathrm{T}_{ph}^{EM}\right]$ is the transform between the Z-string phantom and the MTS coordinate space (obtained based on the "world calibration" using the registration divots); $\{\mathrm{X}_{ph}\}$ represents the coordinates of the intersection points between the US beam and Z-strings in the phantom's coordinate space; $\left[\mathrm{T}_{tool}^{EM}\right]$ is the pose of the US probe with respect to the MTS coordinate system (provided by the MTS); and, lastly $\{\mathrm{X}_{US}\}$ represents the coordinates of the string and US beam intersections in the local coordinate space of the US image (Fig. 2). Once this transformation is determined, any subsequent measurements made, or features identified in the acquired US images, can be mapped into the global coordinate system by means of the calibration transform and respective pose of the US transducer. As such, the 2D ICE images of the left atrium can be displayed within the context of the pre-operative model, according to their correct pose.

2.2. Evaluation and Validation

2.2.1. Engineering-Designed Phantoms—To ensure accurate imaging and faithful representation of the imaged structures, several validation studies were conducted. Using two engineering-designed phantoms (a string phantom and a point-source evaluation phantom), target localization accuracy was assessed by comparing the ground truth location of known targets with their transformed coordinates inferred from the US image.

Point-based registration was used to map the MTS to the local coordinate system of the phantom. Following registration, four linear structures and two point-source targets were characterized using a tracked pointer tool. Subsequently, their global coordinates were compared to their coordinates extracted from the acquired 2D US images.

The second evaluation phantom was designed to enable the localization of point-source targets that resemble surgical instruments (i.e., the tip of a therapy catheter) represented by a 1.5 mm needle-head and a 3 mm metallic sphere, both mounted above a small piece of sound-absorbing material (Sorbothane). Moreover, a 30 mm rubber sphere was also incorporated in the evaluation phantom in order to assess the 2D and 3D geometry characterization of the tracked 2D US. Following registration of the MTS coordinate system into the local coordinate system associated with the evaluation phantom, the 3D sphere of known dimension was scanned in a fan-like fashion and sequential 2D images containing circular cross-sections were acquired. The image acquisition consisted of 20 – 25 frames, which were then individually analyzed. The circular contours were manually outlined, and the selected coordinates were transfered from the coordinate system of the 2D US image into the global 3D coordinate system. The enclosed geometry was reconstructed by interconnecting the elements of the point cloud using the convex hull approach, which was then used to estimate the volume of the reconstructed geometry.

2.2.2. Clinically-emulating Phantom—Subsequently, using a patient-specific left atrial Pt-Si phantom,[13] clinically-emulating evaluation studies were conducted following a methodology that closely mimics the clinical procedure workflow. The phantom is highly representative of patient left atrial anatomy, as it is built using rapid prototyped 3D molds generated from high-quality CT pre-operative images of patient's heart (Fig. 3). Moreover, clinically relevant surgical targets, represented by nylon fiducials, were implanted within the endocardial surface of the phantom. Following registration of the phantom to its CT image and volume-rendered model counterpart, the locations of the nylon implants inferred for the acquired tracked 2D US images were assessed against their true locations in the global coordinate system. This study confirms that representative surgical targets inside the left atrium, or surgical instruments, can be localized with sufficient accuracy in the acquired 2D US images.

3. RESULTS

3.1. Target Localization Error Assessment

Following calibration of the ICE probe, several image acquisition protocols were repeated and the summary of the validation experiments are reported in Table 1. The tracked probe demonstrated consistent target localization accuracy within the clinical requirements (typically under 5 mm accuracy), as well as within the limitations of the system (typically, the MTS accuracy is on the order of 2 mm, and up to 2.5 mm in the laboratory environments).

Fig. 4 shows the target localization accuracy measured in the string phantom. Four linear strings were imaged at six distinct locations along their length and the recorded string coordinates extracted from the 2D US images were transformed into the global coordinate system and evaluated according to their distance from the string (i.e., shortest distance from a point to a line in 3D space). Moreover, two sets of intersecting strings were also imaged (i.e., string intersection was identified by panning across the string intersection until the two string traces can no longer be resolved in the image) and assessed against their ground truth location characterized by repeated measurements using a tracked pointer.

A similar protocol was followed to estimate the localization accuracy of coarser targets (i.e., 1.5 mm needle tip and 3 mm sphere) in the evaluation phantom, which are representative of surgical instruments which are to be identified during image-guided therapy (i.e., catheter tip, guide-wire etc). Fig. 5 shows the target localization accuracy measured at each of the two point source targets. Their coordinates were identified as the center of their trace in the 2D US image, transformed into the global coordinate system using the calibration transform and pose of the probe. The measured coordinates were then assessed against the ground truth location characterized according to the geometry of the phantom and also using a tracked pointer.

Lastly, the nylon fiducials implanted within the Pt-Si phantom were localized using the tracked 2D US probe. However, their identification in the US images was challenging due to the low contrast between the nylon and the surrounding “tissue” mimicking material, which in turn led to a less accurate localization (Fig. 6).

3.2. Volume Reconstruction Assessment

In addition to characterizing the target localization error of known structures and features, another study consisted of evaluating the geometric characterization of known structures based on their images acquired using the tracked US probe. Fig. 7 shows an example of a reconstructed volume based on the convex hull approximation of the point cloud obtained from the sequence of tracked 2D US images, as well as the distribution of the 13 experimentally reconstructed volumes relative to the measured volume of the rubber sphere.

4. DISCUSSION

Here we describe the evaluation of a magnetically tracked 2D intracardiac US probe, which is currently integrated into the prototype system for advanced visualization and image guidance for left atrial ablation treatment.

Two engineering-designed phantoms have been used to assess the probe calibration: a string phantom, containing both linear structures and point source targets, as well as an evaluation phantom consisting of targets that resemble catheter tips of various sizes. In addition, the accuracy with which 2D and 3D geometries can be characterized was also assessed by means of a spherical structure of known dimension.

To address the intended application of the tracked 2D US probe, we also took advantage of a unique and clinically representative phantom based on a patient-specific model of the left atrium to assess the target localization accuracy and the precision with which the structures of interest (i.e., nylon fiducials implanted within the endocardial left atrial surface) can be identified using the tracked 2D images. Such an evaluation is critical to ensure that the imaged features correctly portray the anatomical features and the tracked 2D images are displayed at the correct location and orientation with respect to the pre-operative anatomical models during real-time guidance.

As demonstrated in these studies, the achieved target localization accuracy was consistently on the order of 2–4 mm, under the inherent limitations of the technology employed. The root-mean square (RMS) accuracy of the magnetic tracking system averages 1.5 mm, although in the laboratory settings, it has been shown to be as high as 2 – 2.5 mm,[14] due to magnetic interference with nearby equipment, leading to inhomogeneities in the magnetic field and hence slight tracking errors.

From an imaging standpoint, additional errors are introduced due to the variations between the speed of sound in the media in which the experiments have been performed (i.e., speed of sound in water is typically ~ 1500 m/s), and that used by the US machines to approximate the speed of sound in soft tissue, which is typically 1540 m/s.

Furthermore, the characterization of structures perpendicular to the US beam is also known to be poor, mainly due to the finite thickness of the US fan. The common assumption is that the US fan is an infinitely thin plane which intersects the feature of interest at a well-defined point; in reality, the US fan follows a hyperbolic profile with its minimum thickness at the center of the transmit focal zone, therefore leading to the “smearing” or “blurring” of the imaged feature in the direction perpendicular to the beam. The effects of the US fan thickness are mainly visible when imaging point source targets, where the error associated with the direction of space perpendicular to the beam is slightly larger than the in-plane errors.

Additional studies will consist of further validation and left atrial characterization using a dynamic beating heart phantom, as well as the *ex vivo* imaging of a porcine heart, in order to achieve faithful image quality and feature identification in a soft tissue environment.

5. SUMMARY, CONCLUSIONS AND FUTURE WORK

This work demonstrates the successful implementation and application of a previously developed US calibration technique for tracking a 2D intracardiac US probe that is currently integrated into our advanced prototype system for image guidance and visualization of left atrial ablation therapy. These results suggest that features of interest can be identified and localized using the tracked images with a less than 5 mm error. Together with the high-resolution images of the patient’s left atrium, the 2D US images provide the necessary navigation and real-time positioning feedback to enable precise targeting of the sites to be treated.

In the current setup, the magnetic tracking sensor is rigidly attached to the 2D US transducer and while it serves the purpose for its accuracy evaluation in a laboratory setting, this approach needs to be re-engineered for future animal and patient studies. More efficient means of integration of the magnetic sensor and ICE probe will be explored, and an accuracy vs. seamless integration trade-off can be expected (i.e., the integrated magnetic sensor and US transducer may provide a seamless integration into the procedure workflow, however at the expense of lower accuracy).

Acknowledgments

The authors thank Jon Camp, Bruce Cameron and Ron Karwoski for their software support and Kurt Augustine and Sushravya Raghunath for their help with data acquisition. We also acknowledge funding for this work from the National Institutes of Health (NIH), National Institute of Biomedical Imaging and Bioengineering (NIBIB) Grand No. R01EB002834, National Heart, Lung and Blood Institute (NHLBI), and the Natural Sciences and Engineering Research Council of Canada (NSERC).

References

1. Haissaguerre M, Jais P, Shah DC, Gencel L, Pradeau V, Garrigues S, Chouairi S, Hocini M, Le Métayer P, Roudaut R, Clémenty J. Right and left atrial radiofrequency catheter therapy of paroxysmal atrial fibrillation. J Cardiovasc Electrophysiol. 1996; 7:1132–44. [PubMed: 8985802]
2. Dong J, Dickfeld T, Lamiy SZ, Calkins H. Catheter ablation of atrial fibrillation guided by registered computed tomographic image of the atrium. Heart Rhythm. 2005; 2:1021–2. [PubMed: 16171765]
3. Dickfeld T, Calkins H, Bradley D, Solomon S. Stereotactic catheter navigation using magnetic resonance image integration in the human heart. Heart Rhythm. 2005; 2:413–5. [PubMed: 15851346]
4. Sra J, Krum D, Belanger B, Vaillant R. Registration of 3D left atrial computed tomographic images with fluoroscopy. Heart Rhythm. 2005; 2:1020–2. [PubMed: 16171764]
5. Rettmann M, Holmes DR III, Cameron B, Robb RA. An event-driven distributed processing architecture for image-guided cardiac ablation therapy. Comput Methods Programs Biomed. 2009; 95:95–104. [PubMed: 19285747]
6. Johnson S, Packer DL. Intracardiac ultrasound guidance of multipolar atrial and ventricular mapping basket applications. J Am Coll Cardiol. 1997; 29:202A. [PubMed: 8996315]
7. Rohling R, Munger P, Hollerbach JM, Peter T. Comparison of relative accuracy between a mechanical and an optical position tracker for image-guided neurosurgery. J Image Guid Surg. 1995; 1:30–4. [PubMed: 9079424]
8. Wiles AD, Thompson DG, Frantz DD. Accuracy assessment and interpretation for optical tracking systems. Proc SPIE Medical Imaging 2007: Visualization, Image-Guided Procedures and Display. 2004; 5367:421–32.
9. Schicho K, Figl M, Donat M, Birkfellner W, Seemann R, Wagner A, Bergmann H, Ewers R. Stability of miniature electromagnetic tracking systems. Phys Med Biol. 2005; 50:2089–98. [PubMed: 15843738]
10. Gobbi DG, Comeau RM, Peters TM. Ultrasound probe tracking for real-time ultrasound/MRI overlay and visualization of brain shift. Proc Med Image Comput Comput Assist Interv, Lect Notes Comput Sci. 1999; 1679:920–927.
11. Comeau R, Sadikot AF, Fenster A, Peters TM. Intraoperative ultrasound for guidance and tissue shift correction in image-guided neurosurgery. Med Phys. 2000; 27:787–800. [PubMed: 10798702]
12. Khamene A, Sauer F. A novel phantom-less spatial and temporal ultrasound calibration method. Proc Med Image Comput Comput Assist Interv, Lect Notes Comput Sci. 2004; 3750:671–78.
13. Holmes DR III, Rettmann M, Cameron B, Camp J, Robb R. Developing patient-specific anatomic models for validation of cardiac ablation guidance procedures. Proc SPIE Medical Imaging. 2008; 6918:69181W–8.
14. Kwartowitz DM, Rettmann ME, Holmes DR III, Robb RA. A novel technique for analysis of accuracy of magnetic tracking systems used in image guided surgery. Proc SPIE Medical Imaging 2007: Visualization, Image-Guided Procedures and Modeling. 2010; 7625:76251L1–10.

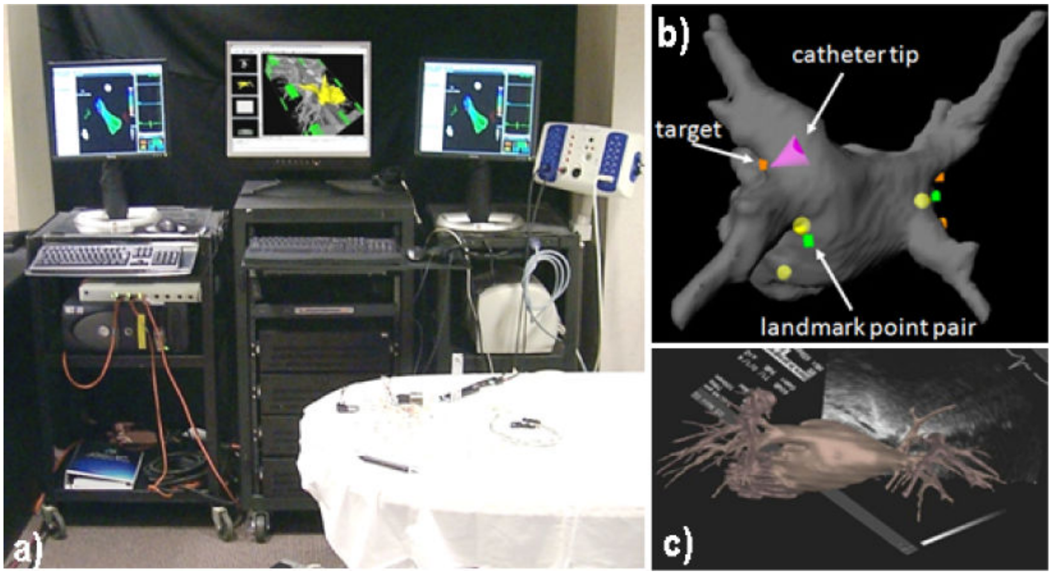

Figure 1.
a) Prototype system for advanced image-guidance and visualization for left atrial ablation therapy; b) Virtual guidance environment showing the registration landmarks, catheter tip and surgical target (*Adapted from Rettmann et al.: Comput Methods Programs Biomed 2009*); c) Example of a tracked 2D US image displayed in the context of the left atrial model.

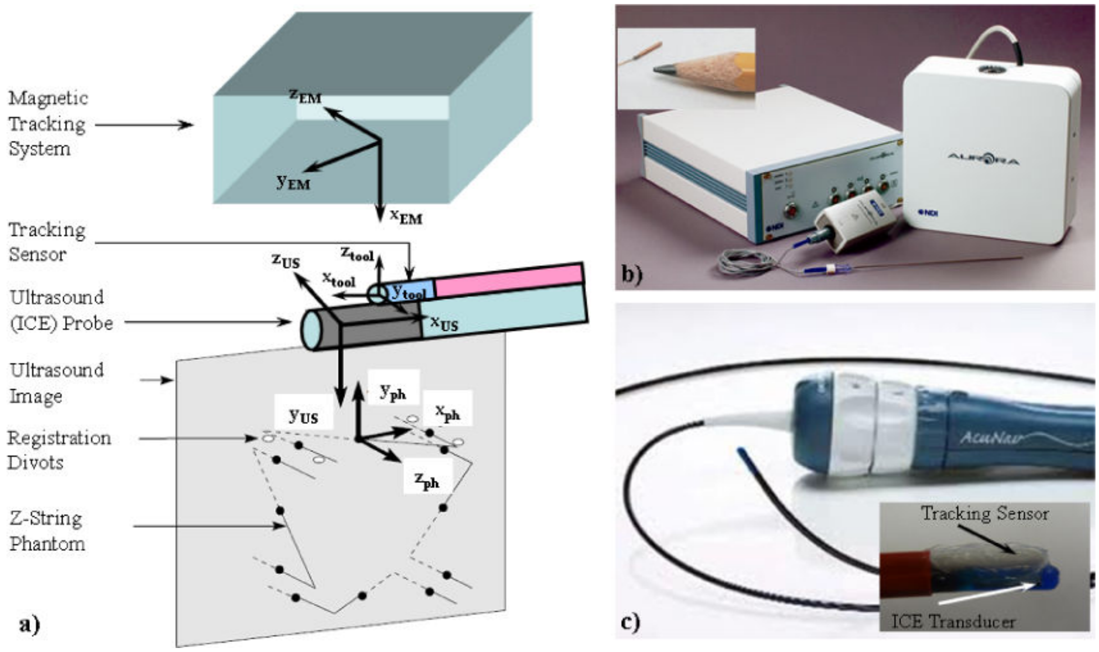

Figure 2.

a) Schematic representation of the US calibration procedure using the Z-string phantom; b) NDI Aurora magnetic tracking system used to track the US transducer for this application; c) ICE probe with a 6 degree-of-freedom NDI Aurora sensor is attached near the tip.

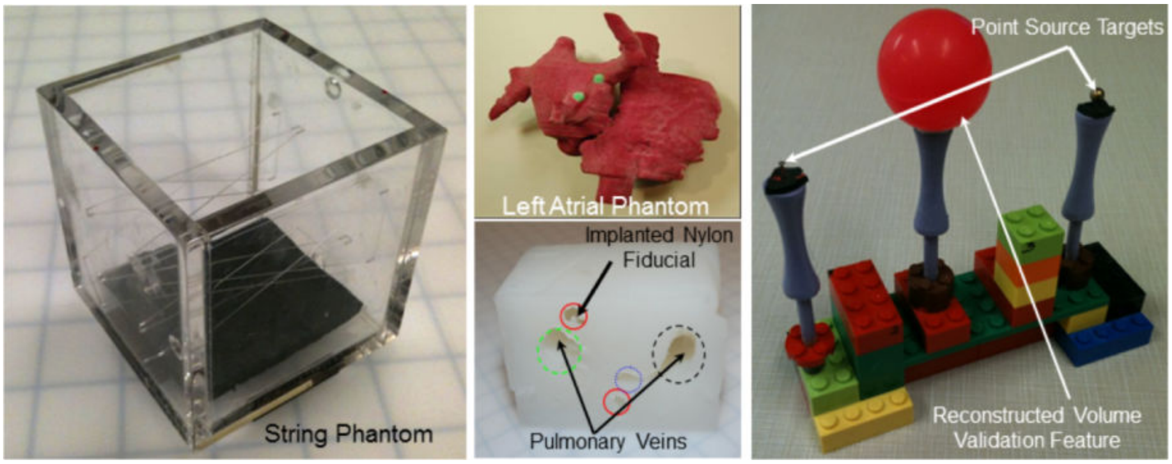

Figure 3.

Engineering-designed phantoms (left and right panels) and clinically-emulating left atrial phantom (middle panel) employed to assess target localization error based on tracked 2D US images. String phantom (left panel) provides a means of characterizing both point-source and linear features; the evaluation phantom (right panel) enables the characterization of features that resemble a therapy catheter tip; lastly, the left atrial Pt-Si phantom — 3D rapid-prototype mold (upper panel) used to build the hollow Pt-Si phantom (lower panel) — incorporates nylon fiducials representing "surgical targets" which can be localized using the traced 2D US images.

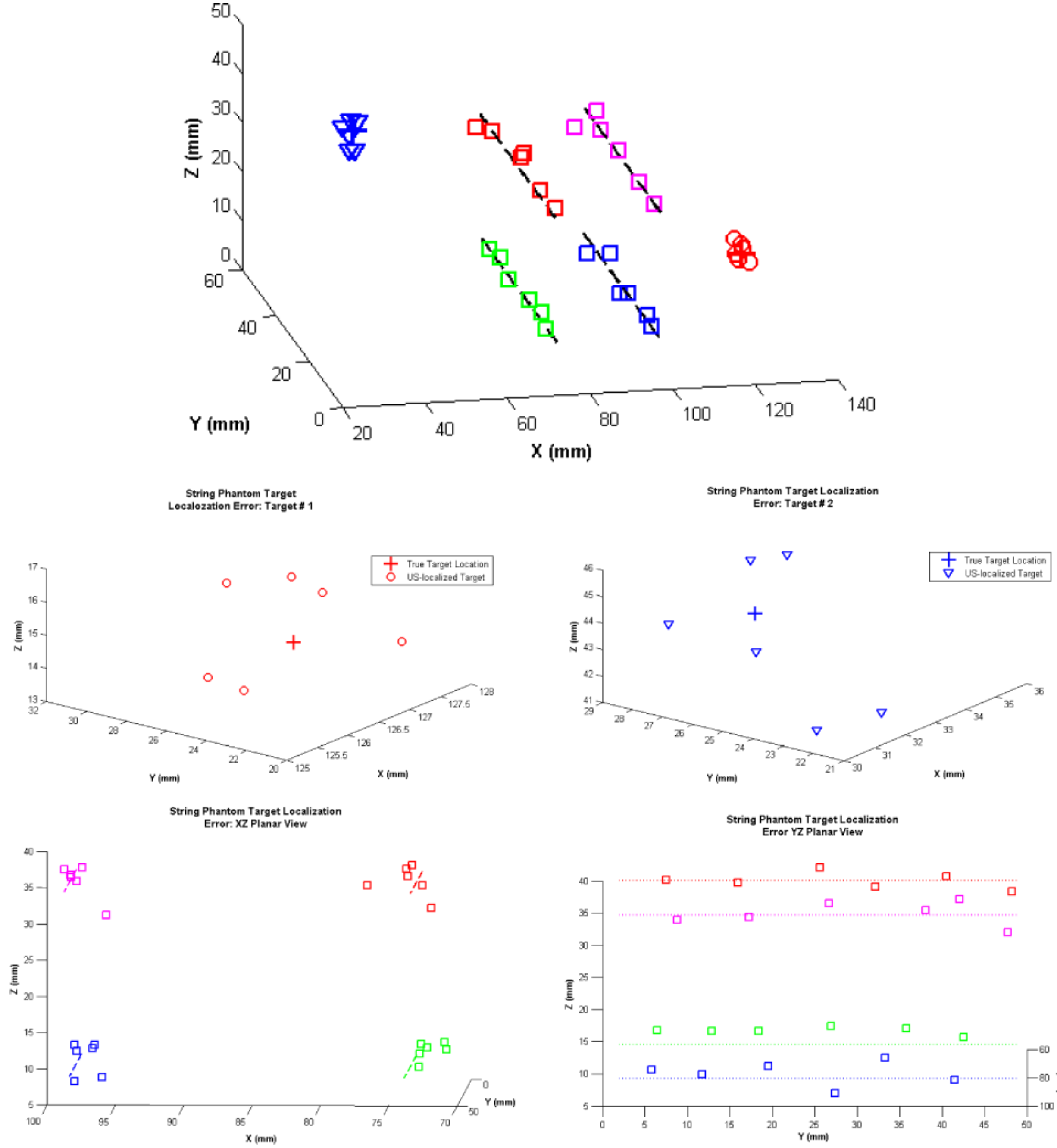

Figure 4.

Target localization accuracy assessed in a nylon string phantom. Two cross-strings targets and four linear structures were characterized based on their images in the tracked 2D US images. Each feature was characterized by 6 images and a localization error on the order of 2 – 4 mm was observed. Lower panels provide a two-dimensional view of the localization error associated with the characteriation of linear features.

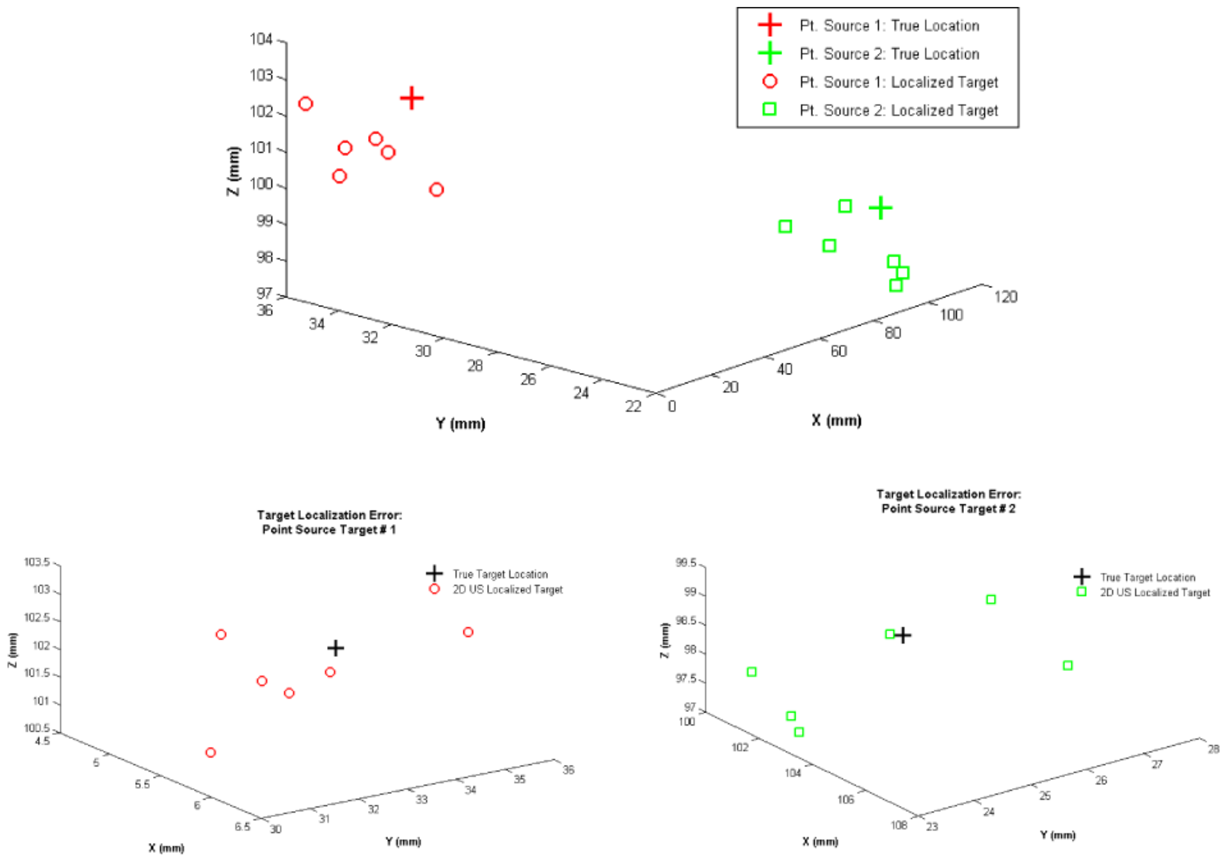

Figure 5.

Point-source (1.5 mm needle-tip and 3 mm sphere) target localization error. Each point source was imaged six times and its global coordinates inferred from the US images are displayed relative to the true target location. Note that the measured target coordinates were within 3 mm of the corresponding ground truth.

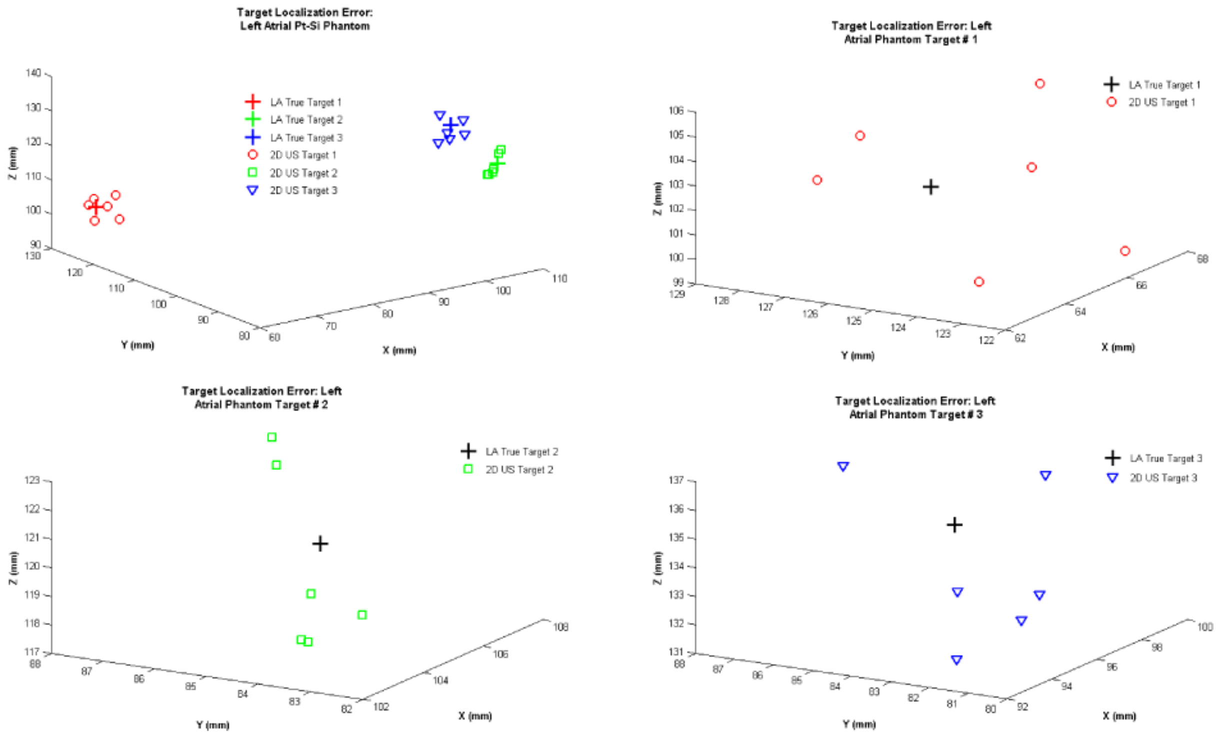

Figure 6.

Fiducial localization error within left atrial-emulating phantom. Each implanted nylon fiducial was imaged six times and its global coordinates inferred from the US images are displayed relative to the true target location. Note that the measured target coordinates were within 2 – 4 mm of the corresponding ground truth.

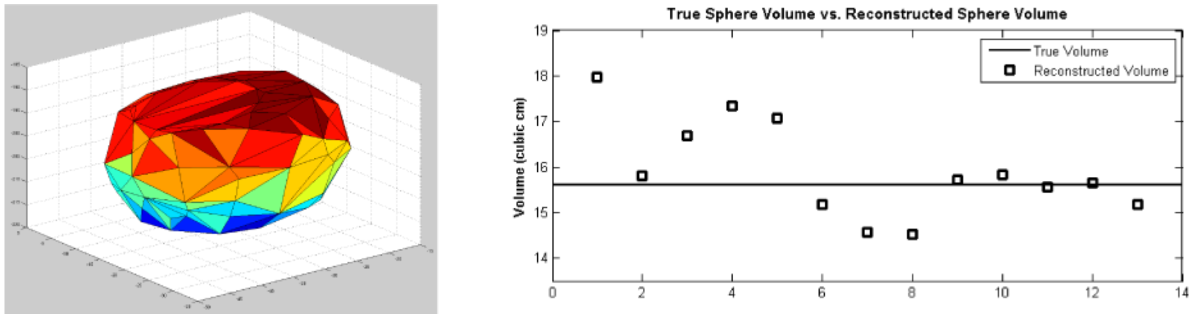

Figure 7.

Reconstructed volume assessment based on the convex hull approximation of the point cloud extracted from sequential acquisition of tracked 2D US images (left panel); Plot showing the true volume and the reconstructed volumes based on 13 acquired image sequences (right panel). Note: the colorbar in the left panel does not represent a measure of reconstruction error, it represents the elevation *Z*) above the *xy* pane.

Table 1

Target Localization Accuracy achieved using a magnetically tracked 2D intracardiac echocradiography (ICE) probe and evaluated in two engineering-design phantoms and a left atrial clinical-emulating phantom.

Evaluated Target	Mean Error ± Std. Dev. (mm)	RMS Error (mm)
Linear String Target # 1	2.4 ± 0.7	2.5
Linear String Target # 2	2.1 ± 0.9	2.3
Linear String Target # 3	1.9 ± 1.1	2.2
Linear String Target # 4	1.8 ± 1.5	2.4
Cross String Target # 1	3.9 ± 1.7	4.3
Cross String Target # 2	3.3 ± 2.0	3.9
Point-Source Target # 1	3.8 ± 1.2	4.0
Point-Source Target # 2	3.7 ± 0.8	3.8
Left Atrial Fiducial # 1	3.6 ± 1.0	3.8
Left Atrial Fiducial # 2	3.0 ± 0.8	3.2
Left Atrial Fiducial # 3	3.4 ± 1.6	3.8

Table 2

Absolute volume reconstruction accuracy and percent volume reconstruction error evaluated in an engineeringdesign phantom using an intracardiac echo (ICE) probe.

Volume Assessment	Measurement
Ground Truth Volume	15.6 cm^3
Reconstructed Absolute Volume	15.9 ± 1.05 cm^3
Percent Error	4.96% ± 4.65%